Journal of Alloys and Compounds 911 (2022) 165034

Contents lists available at ScienceDirect

Journal of Alloys and Compounds

journal homepage: www.elsevier.com/locate/jalcom

Pressure dependent magnetic properties on bulk $CrBr_3$ single crystals

Rubyann Olmos[a], Shamsul Alam[a], Po-Hao Chang[a], Kinjal Gandha[b], Ikenna C. Nlebedim[b], Andrew Cole[c], Fazel Tafti[c], Rajendra R. Zope[a], Srinivasa R. Singamaneni[a,*]

[a] Department of Physics, The University of Texas at El Paso, El Paso, TX 79968, USA
[b] Ames Laboratory, Ames, IA 50011, USA
[c] Department of Physics, Boston College, Chestnut Hill, MA 02467, USA

ARTICLE INFO

Article history:
Received 30 November 2021
Received in revised form 8 April 2022
Accepted 12 April 2022
Available online 21 April 2022

Keywords:
Magnetic measurements
Van der Waals crystal
Magnetization
High-pressure

ABSTRACT

The van der Waals class of materials offer an approach to two-dimensional magnetism as their spin fluctuations can be tuned upon exfoliation of layers. Moreover, it has recently been shown that spin-lattice coupling and long-range magnetic ordering can be modified with pressure in van der Waals materials. In this work, the magnetic properties of quasi two-dimensional $CrBr_3$ are reported applying hydrostatic pressure. The application of pressure up to 0.844 GPa shows a 1.77% decrease in saturation magnetization with a decrease in the Curie temperature from 33.05 to 30.41 K. Density functional theory calculations with pressure up to 1 GPa show a reduction in volume and interplanar distance as pressure increases. To further understand the magnetic properties with applied pressure, the magnetocrystalline anisotropy energy (MAE) and exchange coupling parameter(s) (J) are calculated. There is small decrease in MAE and the first nearest neighbor interaction (J_1) (U = 2.7 eV and J = 0.7 eV) is increasing with respect to increasing pressure. Overall, $CrBr_3$ displays ferromagnetic interlayer coupling and the calculated exchange coupling and MAE parameters match well with the observations from the experimental work.

1. Introduction

Van der Waals (vdW) materials have proven to be promising candidates for magnetoelectronic, data storage, and memory applications [1–4]. Moreover, bulk magnetoelectrical properties and structural characteristics of the CrX_3 (X = Cl, Br, I) and $CrYTe_3$ (Y = Si, Ge) have been amply studied in the literature since two-dimensional (2D) ferromagnetic (FM) ordering was observed in CrI_3 and $Cr_2Ge_2Te_6$, following the fruitful discovery of graphene [2,5–8]. This significant investment placed into the study of vdW materials is by and large due to their ability to retain long-range magnetic ordering down to the low dimensions [1,2,9,10]. Markedly, the weak interlayer bonding present in vdW crystals have allowed scientists to exfoliate or synthesize these materials to one or few layers despite theoretical limitations regarded in the Mermin-Wagner theorem [9]. The key component credited with the stabilization of magnetic ordering in vdW magnets is the uniaxial magnetic anisotropy [2,5,10], thereby allowing long-range magnetic ordering in an isotropic Heisenberg system to exist in the two-dimensions.

The CrX_3 family are exfoliable semiconductors with strong magnetic properties originating from their crystalline structure. In particular, the source of magnetic anisotropy arises from an increase in spin orbit coupling associated with the halogen atom as one moves down the periodic table. Therefore, the magnetocrystalline anisotropy energy (MAE) in the CrX_3 family serves as a form of counteracting thermal fluctuations. This allows magnon excitation gaps to open, which as a result lift constraints imposed by the Mermin-Wagner theory. $CrBr_3$ not only exhibits FM ordering in the bulk but also in the monolayer limit [5,11–14]. In the bulk form, $CrBr_3$ exhibits phase transitions from a monoclinic $C2/m$ phase at high temperatures to a rhombohedral-trigonal $R3$ phase at very low temperatures. The layers in the compound lay along the ab plane and stack along the c plane where the superexchange mechanism grants strong FM interactions along the easy c-axis. In the CrX_3 family, magnetic ordering temperatures and Cr-Cr distance increase with the size of halogen atom from Cl to Br to I, which allows for direct exchange to weaken. Furthermore, the Cr-X bond becomes more covalent as electronegativity decreases from Cl to Br to I, leading to a strengthening of the superexchange interactions, in this order. In chromium trihalides, Cr^{3+} ions are arranged in a honeycomb network in edge-sharing octahedral coordination by six X–ions, each

* Corresponding author.
E-mail address: srao@utep.edu (S.R. Singamaneni).

https://doi.org/10.1016/j.jallcom.2022.165034
0925-8388/

bonded to two Cr ions. The resulting slabs of composition CrX_3 are stacked with vdW gap separating them.

The application of hydrostatic pressure offers a disorderless approach in tuning the magnetic and electrical properties of vdW materials. Moreover, when pressure is applied to a vdW system of weakly coupled layers the bond-angle, interlayer coupling, layer separation and stacking order are strongly affected. The Goodenough-Kanamori-Anderson rules state that when the angle between magnetic ion-ligand-magnetic ion is θ = 90°, the superexchange interaction is FM. On the other hand, direct exchange is antiferromagnetic (AFM) when θ = 180° [15,16]. Manipulation of the superexchange mechanism has been seen in $Cr_2Ge_2Te_6$ where the Cr-Ge-Cr bond angle diverges from 90° when pressure is increased. This tunes the T_C from 66.6 K at 0 GPa to 60.6 K at 1 GPa [17]. It is possible for pressure to push the bond angle towards 90° favoring a FM state, a possibility for CrI_3 as the Cr-I-Cr bond angle is ~95° [18,19] and similarly for $CrBr_3$ where θ = 95.1° [13]. Remarkably, $CrGeTe_3$ has has been recently used to demonstrate a significant increase in T_C exceeding 250 K for pressures (P) greater than 9 GPa, however, this is accompanied by an initial decrease in its T_C in the range $0 < P < \sim$ 4.5 GPa [20]. The magnetic phase transition for $CrBr_3$ has been reported to be in the range of 32–37 K [12,21–24]. $CrBr_3$ is relatively stable in air making it easier to work with compared to its other CrX_3 family members. Additionally, $CrBr_3$ shows interesting magnetic characteristics such as a temperature dependent magnetization and 2D magnetic correlations [25,26].

There are few works in the literature reporting on the pressure-induced magnetic properties of the bulk $CrBr_3$ compound [22,23]. In an initial experimental report, it is observed that T_C decreases with increasing pressure (up to ~11 kbar), however, there was no discussion on how pressure changes magnetization [22]. Recent work by Fumega et al. [23] reports linearly increasing magnetization and a decreasing trend in T_C upon the application of pressures up to 1 GPa. Calculations from Fumega et al. also reveal that the Cr-X-Cr bond angle decreases towards ~ 92° at pressures that reach up to 10 GPa. To broaden the knowledge and understanding of how pressure affects the magnetic properties of $CrBr_3$, we employed experimental and theoretical approaches to study the magnetic properties up to 1 GPa.

2. Methodology

2.1. Experimental

Single crystal samples of $CrBr_3$ were prepared using chemical vapor transport by placing powders of Cr metal and $TeBr_4$ inside a quartz tube and maintaining the hot and cold zones at 700 and 600 °C for 5 days. The green plate-like crystals are a few millimeters across and 50 μm thick [27,28]. Magnetic measurements were performed using a Quantum Design MPMS 3 SQUID magnetometer. Isothermal magnetization measurements were taken at 2 K with a ± 7 T magnetic field. Zero-field cool (ZFC) temperature dependent magnetization was performed from 2 to 150 K with a measuring field of 500 Oe. Hydrostatic pressure was applied using a BeCu Quantum Design piston cell. The pressure transmitting medium was Daphne oil and a Pb manometer was used to monitor the pressure in the cell. Compression of the cell length was increasingly applied and only depressurized after the data collection was completed. See supplemental information [29] for details on assembly of the pressure cell and calculation of the pressure inside the cell.

2.2. Computational details

The optimization of the crystal structures of $CrBr_3$ were carried out with Vienna ab initio (VASP) code [30,31] within projector augmented-wave (PAW) method [32,33]. Generalized gradient approximation (GGA) in the Perdew-Burke-Enzerhof (PBE) [34] method was used for the exchange correlation functional. The non-local vdW functional in form of optB88-vdW [35,36] is incorporated to account for the interlayer vdW force. The plane-wave cut-off energy is 500 eV, and an 8 × 8 × 3 k-point is used to sample the Brillouin zone [37]. For the magnetic property calculations, the on-site Coulomb interactions are taken into account using LDA+U [38] to improve the description of the interactions between localized d electrons of transition atoms. The hydrostatic pressure effect calculation was done by adding the PSTRESS [39] tag, which adds the stress to the stress tensor and an energy generated from the external pressure. All the lattice constants and ionic coordinates were relaxed until the maximum force on all ions is less than 5×10^{-3} eV/Å.

The electronic structure calculations for the magnetic properties are carried out using the pseudo-atomic orbital based [40] OpenMX code [41]. The core electrons are replaced with norm-conserving pseudopotential [42,43] with energy cutoff 200 Ry. The 7 × 7 × 3 k-point mesh was used for BZ integration. On-site Coulomb interactions are particularly strong for the localized d electrons in the $CrBr_3$ system. To remedy this shortcoming in this correlated system, the Hubbard-U method pioneered by Anisimov et al. is applied [44,45]. In treating the localized d-electron states from Cr, we use parameters U = 2.7 eV and J = 0.7 eV taken from Ref. [46] which have also been used in previous studies [47–49]. The Green's function method [50] implemented in OpenMX 3.9 [51] was used to calculate exchange coupling constants J_i for up to the 3rd nearest neighbor (NN). This approach allows the direct calculation of exchange coupling parameter between any pair of magnetic sites for any inter-pair distance.

For MAE, the charge and spin densities were obtained using a self-consistent calculation without spin-orbit coupling (SOC) and kept fixed in subsequent MAE calculations. The MAE was determined as the difference in the total band energy for the configurations with the magnetization aligned in-plane and out-of-plane, with SOC included [52].

3. Results and discussion

In Fig. 1(a), we present the isothermal magnetization at 2 K collected at various pressures up to 0.844 GPa. A ferromagnetic magnetization signal is observed for all pressures for magnetic fields applied out-of-plane. The saturation magnetization (M_s) transitions from 58.89 (0 GPa) to 57.84 emu/g at 0.844 GPa where the inset of Fig. 1(a) shows an amplified view of the M_s. Fig. 1(b) displays the temperature dependence of magnetization with applied pressure up to 0.844 GPa. The same trend is followed where magnetization is decreasing as the cell is increasingly compressed. Curie temperature (T_C) is extracted from the derivative (dM/dT) of the temperature dependent magnetization data, as seen in Fig. 1(c). The variation of T_C as a function of pressure is also plotted in Fig. 1(d), which shows a monotonic decrease of about 2.6 K at the largest applied pressure. Moreover, if pressure causes the bond angle to deviate away from a 90° for the Cr-X-Cr bond angle, T_C is expected to decrease—weakening the superexchange interaction [15,16]. We do note that after the pressure was released, a zero-pressure measurement showed a larger saturation magnetization (~62 emu/g) than before (~ 59 emu/g) the application of pressure, whereas the T_C does not show any change at all.

To gain further insights on the pressure effect within the 1 GPa range, we performed first-principles calculations examining the structure of $CrBr_3$ and its magnetic properties. In treating the localized d-electron states from Cr, we use parameters U = 2.7 eV and J = 0.7 eV. Fig. 2(a) shows the pressure dependence of the lattice ratio c/a as a function of pressure showing a monotonic decrease up to 1 GPa. Similarly, the volume of the crystal is decreasing with increasing pressure, as seen in Fig. 2(b). This suggests that the pressure is compressing the interatomic layer separation of the lattice. It is

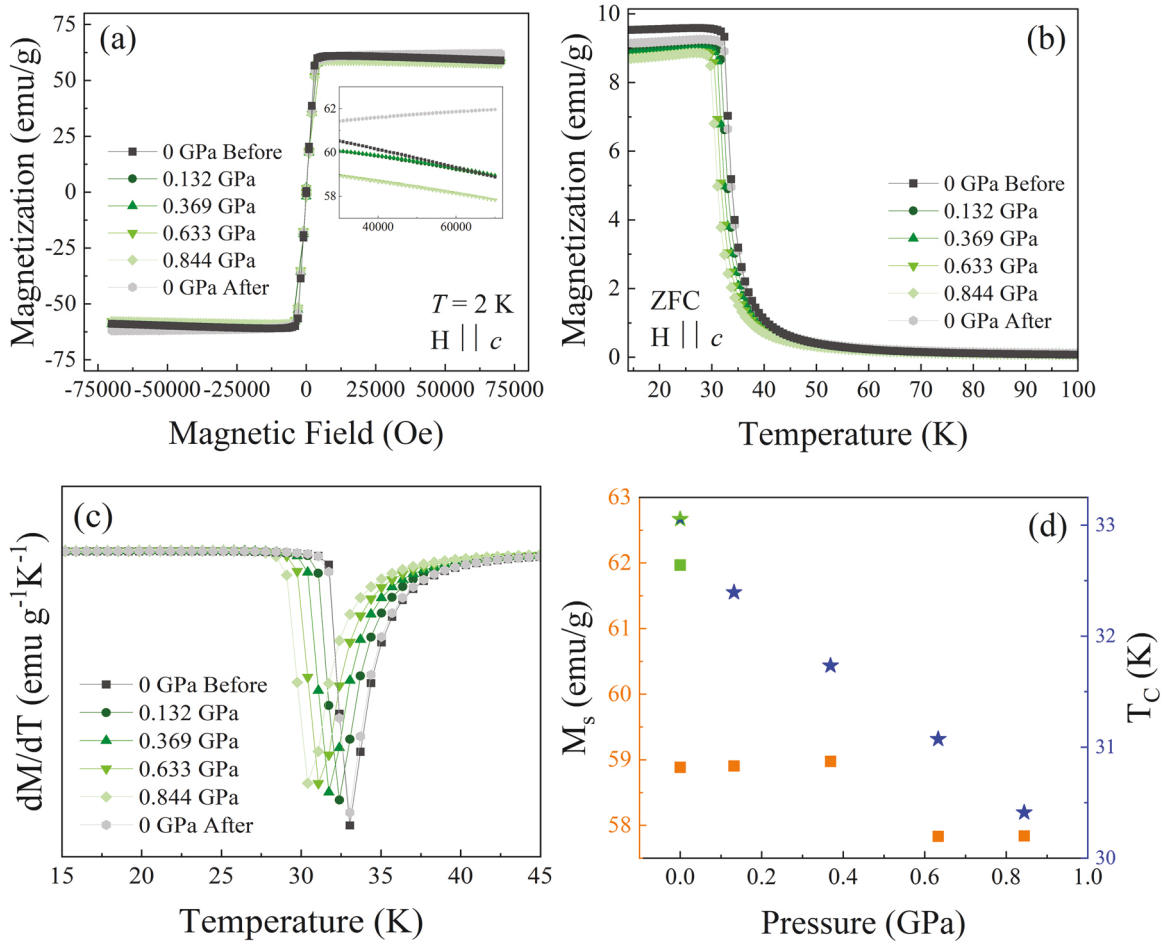

Fig. 1. (a) Isothermal magnetization for pressure up to 0.844 GPa at 2 K with ± 7 T magnetic field. (b) Zero field cool temperature dependent magnetization measurements from 2 to 150 K. (c) Derivative(s) of magnetization with respect to temperature for all pressures. (d) Saturation magnetization, M_s, (left, orange) and Curie temperature, T_C, (right, blue) plotted as a function of pressure where green indicates values at zero pressure upon decompressing the pressure cell from 0.844 GPa.

not surprising that the reduction of *c* is more significant due to weak interlayer coupling. A similar trend is also observed in several other vdW layered systems such as $Cr_2Si_2Te_6$ [17].

To understand how the magnetic properties vary with pressure the exchange coupling *J* and MAE are considered. As discussed in the previous section, the external pressure changes the lattice constants, which influence the inter-site electron hopping process. Two of the main mechanisms that contribute to exchange coupling between the localized moments are direct and super-exchange interactions. It is often the result of the competition between the two that dictates the response of the applied pressure. We employed GF based method to obtain exchange interaction constant J_i (i = 1–3 and *out*) that correspond to up to 3rd NN and the nearest interlayer interaction. This method requires only the ground state and allows a direct calculation of the exchange coupling constant between any given pair of magnetic sites of any distance, which has proven to be more

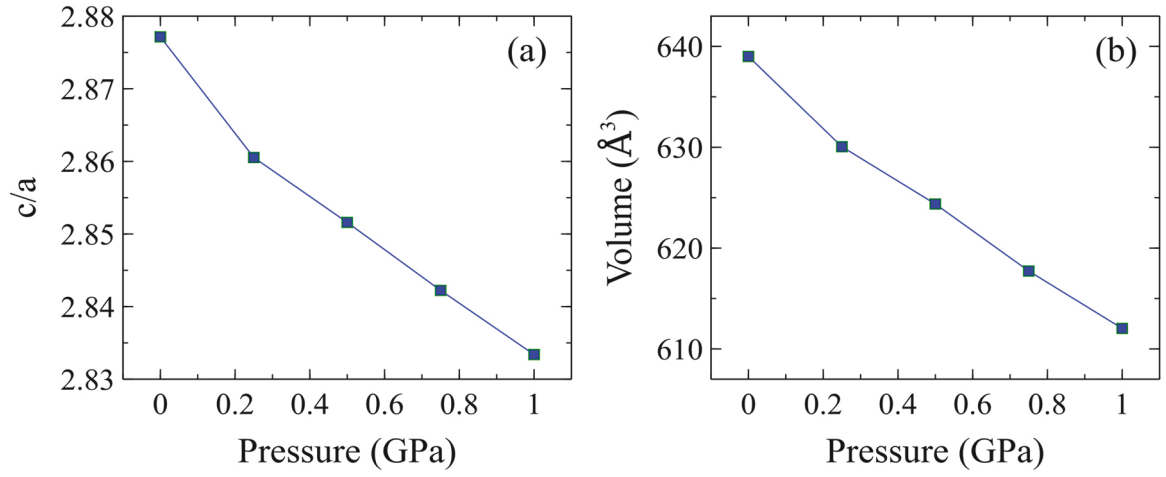

Fig. 2. Theoretical calculations performed as a function of pressure for the (a) lattice parameter ratio c/a and (b) volume.

Table 1
Calculated lattice parameters, volume, and Cr-Cr distance with pressure on.

P (GPa)	a (Å)	c (Å)	c/a (Å)	V (Å)	Cr-Cr (Å)
0.00	6.347	18.236	2.873	636.308	3.668
0.25	6.334	18.116	2.860	629.442	3.658
0.50	6.317	17.994	2.849	621.759	3.651
0.75	6.308	17.928	2.842	617.721	3.642
1.00	6.289	17.821	2.833	610.497	3.634

advantageous for large systems with localized moments [53]. Table 1. shows the values for all J_i evaluated at five different pressures from 0 and 1 GPa with 0.2 increment. The results of J_1 is also plotted in Fig. 3(a) and J_2 and J_{out} due to their energy scale are plotted in Fig. 3(b). J_3 is omitted due to the minuscule contribution. As one can see, in the given pressure range, the only dominant component is the 1st NN interaction J_1 and the interaction strength decreases rapidly as the distance between the pair increases. This is similar to what was suggested by previous studies [54] where both the J_{out} and J_2 are much weaker compared to J_1, particularly under such ambient pressures. Therefore, as our data suggest, they are unlikely to have significant effects on T_C under mean-field consideration.

In our model, we consider the (intra-plane) nearest neighbor exchange interaction J_1. This interaction originates due to the virtual hopping of electrons between the two NN Cr-ions via the Br ion. The super-exchange interaction, due to the presence of the non-magnetic Br atom in between the Cr ions, increases with applied pressure and subsequently, J_1 increases with isothermal compression, see Fig. 3(a). A small but noticeable change due to the applied pressure is seen where J_1 increases almost linearly up to 1 GPa of pressure.

Experimentally [22], a previous report on $CrBr_3$ showed that the T_C decreases from 35.2 K (0 GPa) to approximately 33 K (~1.1 GPa). Such is represented in its negative pressure coefficient (dT_C/dP) = −0.2 K/kbar, implying a negative dependence of J_1 with pressure. From the theoretical perspective, the FM in-plane super-exchange interaction between the Cr^{3+} in bulk $CrBr_3$ appears to be more dominant than the direct exchange (AFM) interaction, which leads to the increase of J_1 with pressure in our calculation. In the experiment in Ref. [22], H. Yoshida claims that the exchange interaction becomes stronger with decreasing atomic distance as there are stronger orbital overlaps. For example, Br has a smaller atomic radius (114 pm) than that of its neighbor I (133 pm), which can contribute to the dominant Cr-Cr direct exchange interaction. Combining all these effects, the competition between the direct exchange and the indirect super-exchange interaction determines the nature of the J_1 dependence with pressure for $CrBr_3$. The competition between AFM

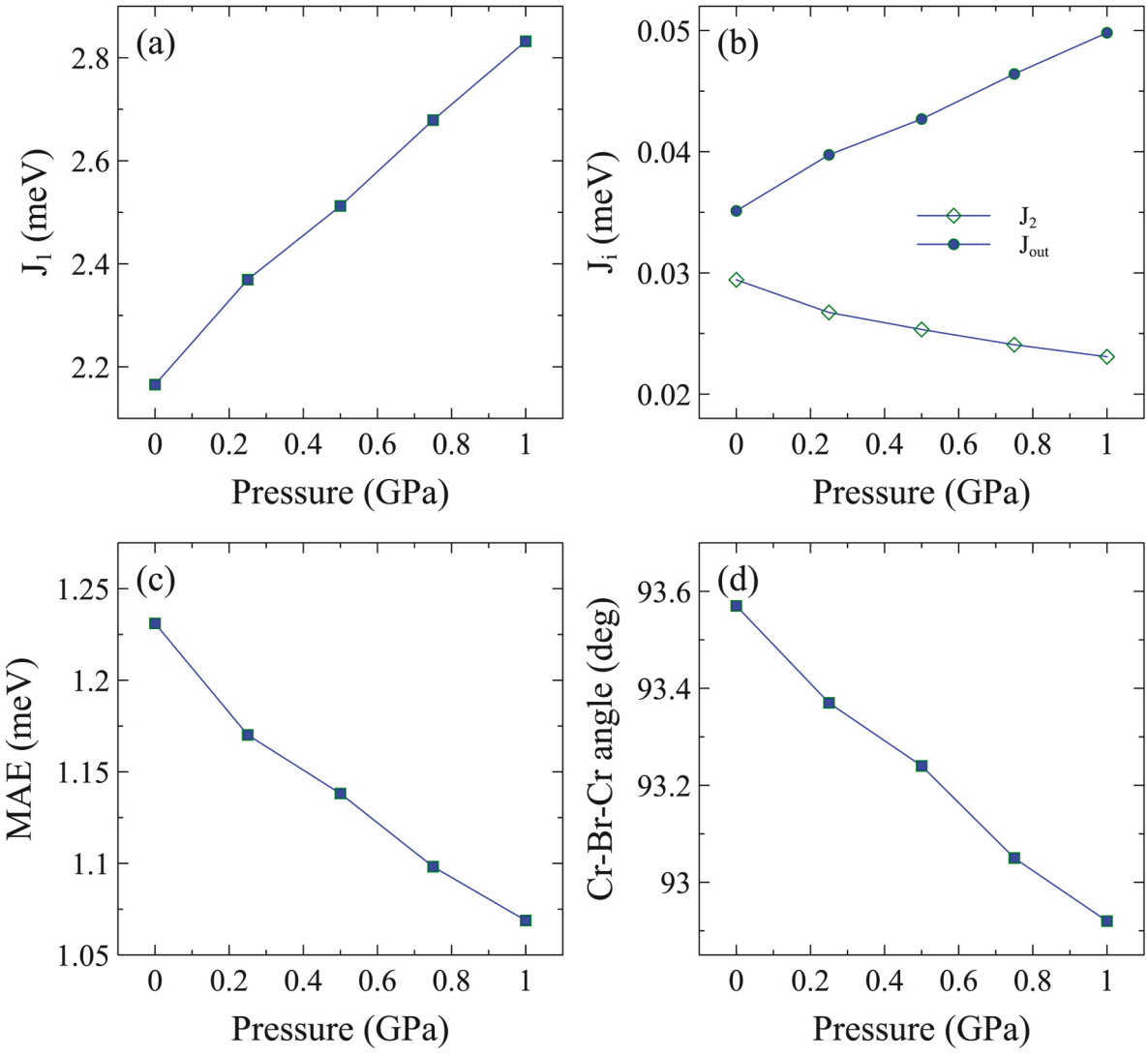

Fig. 3. (a) Calculated first nearest neighbor exchange coupling parameter J_1 up to 1 GPa. (b) Second nearest neighbor, J_2, and J_{out} as a function of increasing pressure. (c) Calculated magnetocrystalline anisotropy energy as a function of hydrostatic pressure. (d) Reduction of the Cr-Br-Cr bond angle as pressure is increasing.

direct exchange through Cr–Cr bonding, and FM super-exchange through Cr–Br–Cr bonding, are what determine the nature of the J_1 dependence with pressure for $CrBr_3$.

The pressure dependence of MAE is shown in Fig. 3(c). At $P = 0$, MAE is about 200 μeV/Cr, similar to that of single layer $CrBr_3$ from a previous theoretical study [18,55]. The overall result also shows a similar pressure dependent trend to monolayer $CrBr_3$ under strain in terms of intra-plane distance where the MAE decreases as bond length reduces due to increasing pressure. When comparing $CrBr_3$ to CrI_3, for example, the Cr-Cr separation increases with expanding halogen size from Br to I, as a result direct exchange (overlap between neighboring Cr orbitals) weakens successively enhancing the covalent nature of the Cr-X bond [56]. It is important to note that the change in bond angle, Fig. 3(d), and the increase in interlayer coupling, Fig. 3(a), could give rise to larger T_C if the system goes to higher pressures. An interesting case has recently been seen for $CrGeTe_3$ where T_C initially decreases with increasing pressure, then significantly increases above 250 K at pressures above 9.1 GPa [20]. Therefore, the relationship of MAE and T_C might not be consistent with the general trend observed in $CrBr_3$ warranting further investigations into the magnetic behavior at pressures greater than 1 GPa.

It is important to point out that the theoretical explanation of pressure dependence of exchange coupling on chromium halides is still controversial and debatable [56]. It is known that such type of systems possesses localized *d*-electrons, which are strongly correlated, and pure DFT is inadequate. As a result, an additional correction U to onsite Coulomb interaction is necessary [46,57]. However, the popular LDA+U method, which has been widely adopted in many previous studies, is only able to produce correct pressure dependent trend for exchange coupling of certain systems in the chromium (i.e. CrI_3) halide family and fail at the others. For example, T_C for CrI_3 and $CrBr_3$ are experimentally observed to have the opposite pressure dependency. However, theoretically, DFT+U approach predicts both to have similar trend as T_C increases with pressure in both cases. This is possibly due to the limit of the empirical nature of the method.

4. Conclusion

In this work, we used pressure as the tuning parameter to explore the magnetic characteristics of the less studied chromium trihalide, $CrBr_3$. We reveal through experiment that M_s and T_C both decrease upon increasing the pressure up to 0.844 GPa. Moreover, our computations realize that the role of pressure on J values is very complicated and gives rise to further questions, especially considering that there are a very few pressure-induced calculations and experiments performed on the bulk $CrBr_3$ system. Although, T_C was not drastically altered for the bulk $CrBr_3$ case, recent works have shown the importance of carrying out pressure dependent studies at significantly higher pressures. Thus, it is important to fully characterize the pressure dependent magnetic properties of $CrBr_3$ at pressures above 1 GPa in the future.

CRediT authorship contribution statement

Rubyann Olmos: Conceptualization, Data curation, Investigation, Writing – original draft, Writing – review & editing. **Shamsul Alam:** Theory, Investigation, Data curation. **Po-Hao Chang:** Theory, Data curation, Writing – review & editing. **Kinjal Gandha:** Data curation, Resources. **Ikenna C. Nlebedim:** Data curation, Resources. **Andrew Cole:** Resources. **Fazel Tafti:** Resources, **Rajendra R. Zope:** Theory, Writing – review & editing. **Srinivasa R. Singamaneni:** Supervision, Writing – review & editing.

Declaration of Competing Interest

The authors declare that they have no known competing financial interests or personal relationships that could have appeared to influence the work reported in this paper.

Acknowledgments

This material is based upon work supported by the National Science Foundation Graduate Research Fellowship Program under Grant No. 1848741. Any opinions, findings, and conclusions or recommendations expressed in this material are those of the author(s) and do not necessarily reflect the views of the National Science Foundation. S.R.S. and R.O. acknowledge support from the NSF-DMR (Award No. 2105109). SRS acknowledges support from NSF-MRI (Award No. 2018067). PHC and RRZ are supported by the US Department of Energy, Office of Science, Office of Basic Energy Sciences, as part of the Computational Chemical Sciences Program under Award No. DE-SC0018331. Support for computational time at the Texas Advanced Computing Center directly and through NSF Grant No. TG-DMR090071. This work was, in part, performed at Ames Laboratory, operated for the U.S. Department of Energy by Iowa State University of Science and Technology under Contract No. DE-AC02-07CH11358.

Appendix A. Supporting information

Supplementary data associated with this article can be found in the online version at doi:10.1016/j.jallcom.2022.165034.

References

[1] G.A. Prinz, Magnetoelectronics, Science 282 (5394) (1998) 1660.
[2] C. Gong, L. Li, Z. Li, H. Ji, A. Stern, Y. Xia, T. Cao, W. Bao, C. Wang, Y. Wang, Z.Q. Qiu, R.J. Cava, S.G. Louie, J. Xia, X. Zhang, Discovery of intrinsic ferromagnetism in two-dimensional van der Waals crystals, Nat 546 (2017) 265.
[3] M. Wuttig, N. Yamada, Phase-change materials for rewriteable data storage, Nat. Mater. 6 (2007) 824.
[4] W. Zhang, R. Mazzarello, M. Wuttig, E. Ma, Designing crystallization in phase-change materials for universal memory and neuro-inspired computing, Nat. Rev. Mater. 4 (2019) 150.
[5] B. Huang, G. Clark, E. Navarro-Moratalla, D.R. Klein, R. Cheng, K.L. Seyler, D. Zhong, E. Schmidgall, M.A. McGuire, D.H. Cobden, et al., Layer-dependent ferromagnetism in a van der Waals crystal down to the monolayer limit, Nature 546 (2017) 270.
[6] K.S. Novoselov, A.K. Geim, S.V. Morozov, D. Jiang, Y. Zhang, S.V. Dubonos, I.V. Grigorieva, A.A. Firsov, Electric field effect in atomically thin carbon films, Science 306 (2004) 666.
[7] X. Zhang, L. Li, D. Weber, J. Goldberger, K.F. Mak, J. Shan, Gate-tunable spin waves in antiferromagnetic atomic bilayers, Nat. Mater. 19 (2020) 838.
[8] C. Gong, X. Zhang, Two-dimensional magnetic crystals and emergent heterostructure devices, Science 363 (2019) eaav4450.
[9] N.D. Mermin, H. Wagner, Absence of ferromagnetism or antiferromagnetism in one or two-dimensional isotropic Heisenberg models, Phys. Rev. Lett. 17 (1966) 1133.
[10] Z. Fei, B. Huang, P. Malinowski, W. Wang, T. Song, J. Sanchez, W. Yao, D. Xiao, X. Zhu, A.F. May, et al., Two-dimensional itinerant ferromagnetism in atomically thin Fe_3GeTe_2, Nat. Mater. 17 (2018) 778.
[11] M.A. McGuire, H. Dixit, V.R. Cooper, B.C. Sales, Coupling of crystal structure and magnetism in the layered, ferromagnetic insulator CrI_3, Chem. Mater. 27 (2015) 612.
[12] I. Tsubokawa, On the magnetic properties of a $CrBr_3$ single crystal, J. Phys. Soc. Jpn. 15 (1960) 1664.
[13] Z. Zhang, J. Shang, C. Jiang, A. Rasmita, W. Gao, T. Yu, Direct photoluminescence probing of ferromagnetism in monolayer two-dimensional $CrBr_3$, Nano Lett. 19 (2019) 3138.
[14] H.H. Kim, B. Yang, S. Li, S. Jiang, C. Jin, Z. Tao, G. Nichols, F. Sfigakis, S. Zhong, C. Li, S. Tian, et al., Evolution of interlayer and intralayer magnetism in three atomically thin chromium trihalides, Proc. Natl. Acad. Sci. U. S. A. 116 (2019) 11131.
[15] P.W. Anderson, Antiferromagnetism. Theory of superexchange interaction, Phys. Rev. 79 (1950) 350.
[16] J.B. Goodenough, Theory of the role of covalence in the perovskite-type manganites [La, M(II)]MnO_3, Phys. Rev. 100 (1955) 564.
[17] Y. Sun, R.C. Xiao, G.T. Lin, R.R. Zhang, L.S. Ling, Z.W. Ma, X. Luo, W.J. Lu, Y.P. Sun, Z.G. Sheng, Effects of hydrostatic pressure on spin-lattice coupling in two-dimensional ferromagnetic $Cr_2Ge_2Te_6$, Appl. Phys. Lett. 112 (2018) 072409.

[18] L. Webster, J. Yan, Strain-tunable magnetic anisotropy in monolayer $CrCl_3$, $CrBr_3$, and CrI_3, Phys. Rev. B 98 (2018) 144411.
[19] J.L. Lado, J. Fernández-Rossier, On the origin of magnetic anisotropy in two dimensional CrI_3, 2D Mater. 4 (2017) 035002.
[20] D. Bhoi, J. Gouchi, N. Hiraoka, Y. Zhang, N. Ogita, T. Hasegawa, K. Kitagawa, H. Takagi, K.H. Kim, Y. Uwatoko, Nearly room-temperature ferromagnetism in a pressure-induced correlated metallic state of the van der Waals insulator $CrGeTe_3$, Phys. Rev. Lett. 127 (2021) 217203.
[21] L.D. Jennings, W.N. Hansen, Heat capacity of $CrBr_3$ from 14 to 360 °K, Phys. Rev. 139 (1965) 1694.
[22] H. Yoshida, J. Chiba, T. Kaneko, Y. Fujimori, S. Abe, Pressure effect on the Curie temperature of $CrBr_3$, Phys. B 237–238 (1997) 525–526.
[23] A.O. Fumega, S. Blanco-Canosa, H. Babu-Vasili, P. Gargiani, H. Li, J. Zhou, F. Rivadulla, V. Pardo, Electronic structure and magnetic exchange interactions of Cr-based van der Waals ferromagnets. A comparative study between $CrBr_3$ and $Cr_2Ge_2Te_6$, J. Mater. Chem. C. 8 (2020) 13582–13589.
[24] V.A. Alyoshin, V.A. Berezin, V.A. Tulin, rf susceptibility of single-crystal $CrBr_3$ near the Curie temperature, Phys. Rev. B 56 (1997) 2.
[25] N. Richter, D. Weber, F. Martin, N. Singh, U. Schwingenschlögl, B.V. Lotsch, M. Kläui, Temperature-dependent magnetic anisotropy in the layered magnetic semiconductors CrI_3 and $CrBr_3$, Phys. Rev. Mater. 2 (2018) 024004.
[26] C.L. Saiz, J.A. Delgado, J. van Tol, T. Tartaglia, F. Tafti, S.R. Singamaneni, 2D correlations in the van der Waals ferromagnet $CrBr_3$ using high frequency electron spin resonance spectroscopy, J. Appl. Phys. 129 (2021) 233902.
[27] M. Abramchuk, S. Jaszewski, K.R. Metz, G.B. Osterhoudt, Y. Wang, K.S. Burch, F. Tafti, Controlling magnetic and optical properties of the van der Waals crystal $CrCl_{3-x}Br_x$ via mixed halide chemistry, Adv. Mater. 30 (2018) 1801325.
[28] T.A. Tartaglia, J.N. Tang, J.L. Lado, F. Bahrami, M. Abramchuk, G.T. McCandless, M.C. Doyle, K.S. Burch, Y. Ran, J.Y. Chan, F. Tafti, Accessing new magnetic regimes by tuning the ligand spin-orbit coupling in van der Waals magnets, Sci. Adv. 6 30 (2020) eabb9379.
[29] Supplemental information: doi:10.1016/j.jallcom.2022.165034.
[30] G. Kresse, J. Furthmuller, Efficiency of ab-initio total energy calculations for metals and semiconductors using a plane-wave basis set, Comp. Mater. Sci. 6 (1996) 15.
[31] G. Kresse, J. Furthmuller, Efficient iterative schemes for ab initio total-energy calculations using a plane-wave basis set, Phys. Rev. B 54 (1996) 11169.
[32] P.E. Blochl, Projector augmented-wave method, Phys. Rev. B 50 (1994) 17953.
[33] G. Kresse, D. Joubert, From ultrasoft pseudopotentials to the projector augmented-wave method, Phys. Rev. B 59 (1999) 1758.
[34] J.P. Perdew, K. Burke, M. Ernzerhof, Generalized gradient approximation made simple, Phys. Rev. Lett. 77 (1996) 3865.
[35] J. Klimes, D.R. Bowler, A. Michaelides, Van der Waals density functionals applied to solids, Phys. Rev. B 83 (2011) 195131.
[36] J. Klimes, D.R. Bowler, A. Michaelides, Chemical accuracy for the van der Waals density functional, J. Phys.: Conden. Matter 22 (2009) 022201.
[37] H.J. Monkhorst, J.D. Pack, Special points for Brillouin-zone integrations, Phys. Rev. B 13 (1976) 5188.
[38] V.I. Anisimov, O. Gunnarsson, Density-functional calculation of effective Coulomb interactions in metals, Phys. Rev. B 43 (1991) 7570.
[39] ⟨h⟩⟨ttp://cms.mpi.univie.ac.at/VASP/⟩.
[40] T. Ozaki, Variationally optimized atomic orbitals for large-scale electronic structures, Phys. Rev. B 67 (2003) 155108.
[41] T. Ozaki, OpenMX 3.8, ⟨http://www.openmx-square.org⟩.
[42] I. Morrison, D.M. Bylander, L. Kleinman, Nonlocal Hermitian norm-conserving Vanderbilt pseudopotential, Phys. Rev. B 47 (1993) 6728.
[43] D. Vanderbilt, Soft self-consistent pseudopotentials in a generalized eigenvalue formalism, Phys. Rev. B 41 (R) (1990) 7892.
[44] V.I. Anisimov, I.V. Solovyev, M.A. Korotin, M.T. Czyżyk, G.A. Sawatzky, Density-functional theory and NiO photoemission spectra, Phys. Rev. B 48 (1993) 16929.
[45] S. Ryee, M.J. Han, The effect of double counting, spin density, and Hund interaction in the different DFT+U functionals, Sci. Rep. 8 (2018) 9559.
[46] X. Lu, R. Fei, L. Yang, Curie temperature of emerging two-dimensional magnetic structures, Phys. Rev. B 100 (2019) 205409.
[47] J. Liu, Q. Sun, Y. Kawazoe, P. Jena, Exfoliating biocompatible ferromagnetic Cr-trihalide monolayers, Phys. Chem. Chem. Phys. 18 (2016) 8777–8784.
[48] J.L. Lado, J. Fernández-Rossier, On the origin of magnetic anisotropy in two dimensional CrI_3, 2D Mater. 4 (2017) 035002.
[49] P. Jiang, L. Li, Z. Liao, Y.X. Zhao, Z. Zhong, Spin direction-controlled electronic band structure in two-dimensional ferromagnetic CrI_3, Nano Lett. 18 (6) (2018) 3844–3849.
[50] A.I. Liechtenstein, M.I. Katsnelson, V.P. Antropov, V.A. Gubanov, Local spin density functional approach to the theory of exchange interactions in ferromagnetic metals and alloys, J. Magn. Magn. Mater. 67 (1987) 65–74.
[51] A. Terasawa, M. Matsumoto, T. Ozaki, Y. Gohda, Efficient algorithm based on Liechtenstein method for computing exchange coupling constants using localized basis set, J. Phys. Soc. Jpn. 88 (2019) 114706.
[52] P.-H. Chang, W. Fang, T. Ozaki, K.D. Belashchenko, Voltage-controlled magnetic anisotropy in antiferromagnetic MgO-capped MnPt films, Phys. Rev. Mater. 5 (2021) 054406.
[53] N. Episcopo, P.-H. Chang, T.W. Heitmann, K. Wangmo, J. McKamey Guthrie, M. Fitta, R.A. Klein, N. Poudel, K. Gofryk, R.R. Zope, Magnetic structure, excitations and short-range order in honeycomb Na2Ni2TeO6, J. Phys.: Condens. Matter 33 (2021) 375803.
[54] L.J. De Jongh, A.R. Miedema, Experiments on simple magnetic model systems, Adv. Phys. 50 (8) (2001) 947–1170.
[55] W.-B. Zhang, Q. Qu, P. Zhu, C.-H. Lam, Robust intrinsic ferromagnetism and half semiconductivity in stable two-dimensional single-layer chromium trihalides, J. Mater. Chem. C. 3 (2015) 12457.
[56] S. Mondal, M. Kannan, M. Das, L. Govindaraj, R. Singha, B. Satpati, S. Arumugam, P. Mandal, Effect of hydrostatic pressure on ferromagnetism in two-dimensional CrI_3, Phys. Rev. B 99 (18) (2019) 180407.
[57] R. Albaridy, A. Manchon, U. Schwingenschlögl, Tunable magnetic anisotropy in Cr–trihalide Janus monolayers, J. Phys.: Condens. Matter 32 (2020) 355702.